Hydrometallurgy 203 (2021) 105616

Contents lists available at ScienceDirect

Hydrometallurgy

journal homepage: www.elsevier.com/locate/hydromet

Arsenic behavior during the treatment of refractory gold ores via POX: Characterization of Fe-AsO_4-SO_4 precipitates

Jakolien A. Strauss [a], Volha Bazhko [b,*], Genarro Ventruti [c], Xuan Liguo [d], Mario A. Gomez [d,*]

[a] Outotec (RSA) (Pty) Ltd, 3rd Floor, Building 14, Byls Bridge, Centurion 0157, South Africa
[b] Mintek, 200 Malibongwe Dr., Randburg 2194, South Africa
[c] Dipartimento di Scienze della Terra e dell'Ambiente, Università di Bari "Aldo Moro", Via Orabona 4, Bari 70125, Italy
[d] Liaoning Engineering Research Center for Treatment and Recycling of Industrially Discharged Heavy Metals, Shenyang University of Chemical Technology, Shenyang, LN 110142, China

ARTICLE INFO

Keywords:
Iron-arsenic precipitates
Hydrothermal synthesis
Pressure oxidation
Refractory gold
Sulfide concentrates

ABSTRACT

Arsenic is a common contaminant in refractory gold ores/concentrates and it's accepted that total pressure oxidation (POX) is the most appropriate technology to treat these due to their refractoriness and ability to stabilize arsenic via ferric arsenate compounds (Fe-As). However, information gaps about the behavior and stability of the various Fe-As's formed at high temperatures in downstream gold processing steps remain and may have significant practical implications. This paper focuses on the precipitation behavior of arsenic during autoclaving of various arsenopyrite containing ore concentrates from around the world. The first portion involved the precipitation of different synthetic precipitates at POX conditions found in the gold industry by varying Fe/As ratios in the feed solutions. Mineralogical characterization results showed that arsenate-containing basic ferric sulphate (As-BFS), basic ferric arsenate sulphate (BFAS), and ferric arsenate sub-hydrate (FAsH) formed. In the second portion, five pyrite/arsenopyrite concentrates received from gold mines around the world were submitted to batch POX and mineralogical analysis. We observed that the mechanism of precipitation for pyrite/arsenopyrite concentrates appears to be different vs. synthetic solutions. Upon processing of the gold concentrates under POX, the initial Fe/As ratio in the concentrates was retained to the final generated residues. The major Fe-As's generated in the POX residues from the concentrates were As-BFS and BFAS, while non-As containing ferric phases included hematite and some small fraction of jarosite. Finally, we observed that as the Fe/As molar ratio in the concentrate feed increased, the amount of As-BFS decreased while that of BFAS increased.

1. Introduction

Arsenic (As) is a common impurity in refractory gold sulphide ores and concentrates from primary minerals such as arsenopyrite, arsenian pyrite, chalcopyrite, enargite, tennantite, and to lesser extents orpiment and realgar (Adams, 2016; Conner-Mills and Anderson, 2018; Coudert et al., 2019; Twidwell, 2019). Roasting may be applied to refractory gold ores or concentrates and as of 2011, it accounted for ~21% of processing from major global gold producers (Gold Exploration, 2012). However, roasting is deemed unfavorable to treat high arsenic containing gold ores due to toxic gas environmental concerns and economic costs. This is especially true now and in the future as global depletion of high grade and native gold ores with low As occurs (Adams, 2016; Conner-Mills and Anderson, 2018; Coudert et al., 2019; Fernandez et al., 2010; Nan et al., 2014; Twidwell, 2019; Wang et al., 2019; Yaozhong and Smith, 2004). Therefore, the need to treat high As containing Au ores and concentrates to efficiently leach the Au and simultaneously precipitate unwanted elements (e.g. As, Fe, Sb) to produce waste solids that are environmentally stable under several conditions is of the utmost importance. As such total pressure oxidation (POX) leaching under acidic conditions is the preferred option for the pre-treatment of refractory gold ores and concentrates with higher As content (1–10 wt%) due to various processing and environmental benefits (Adams, 2016; Filyanin and Vorobev-Desatovskiy, 2014; Fletcher, 2012; Frostiak and Haugard, 1992; Robins and Jayaweera, 1992).

Under POX acid leaching conditions where typical oxidation

* Corresponding authors.
E-mail addresses: olgab@mintek.co.za (V. Bazhko), mario.gomez@syuct.edu.cn (M.A. Gomez).

https://doi.org/10.1016/j.hydromet.2021.105616
Received 19 January 2021; Received in revised form 20 April 2021; Accepted 27 April 2021
Available online 31 May 2021

acidities (10–50 g/L H_2SO_4) and temperatures (180–230 °C) are used (Adams, 2016), Arsenic-bearing primary minerals undergo complex reactions that may form hematite (Fleuriault, 2016), jarosites (Das et al., 1996), basic ferric sulfate (Cheng and Demopoulos, 2004; Dutrizac, 1987; Fleming, 2009) and a range of possible Fe(III)-AsO_4-SO_4 phases (Dutrizac and Jambor, 2007; Gomez et al., 2008, 2011; Robins and Jayaweera, 1992; Swash and Monhemius, 1994).

The first set of studies on the formation of Fe(III)-AsO_4-SO_4 phases that may form during POX leaching of gold ores and concentrates occurred at the Imperial College in London (Swash and Monhemius, 1994). Effects of temperature (150–225 °C), Fe/As molar ratio [As(V) varied] at a fixed retention time of 24 h were studied. This yielded 4 distinct phases (Table S1) labeled as Basic Ferric Sulphate (BFS), Scorodite (Sc), Type I, and Type II. Later in 2007, CANMET investigated effects of temperature (175–225 °C), time (1–24 h), initial acidity (0–69 g/L H_2SO_4), and Fe/As ratios [both initial Fe(III) and As(V) varied] (Dutrizac and Jambor, 2007). Herein BFS, Sc, and two new phases (Phase 3 and 4) precipitated (Table S1). Recently, McGill's Hydrometallurgical labs and the Università di Bari Aldo Moro investigated effects of temperature (150–225 °C), Fe/As molar ratio [As(V) varied] and time (1–24 h) (Gomez et al., 2008, 2010, 2011, 2013). Four phases were determined (Table S1), confusion about the old and newly formed phases resolved, more explicit chemical names and formulae were given, a new precipitation diagram was determined, and the monoclinic crystal structure of the infamous BFAS/Phase 3/ Type II solid solution was determined and revised (Ventruti et al., 2020). Furthermore, the general reaction which describes the formation of these phases (Table S1) follows:

$$Fe(SO_4)_{1.5} + H_3AsO_4 + (w + z/2)H_2O \rightarrow Fe(AsO_4)x(SO_4)y(OH)z\cdot wH_2O + (1.5 - y)H_2SO_4 \quad (1)$$

Thus from all these works, we can observe that the precipitation and composition of these phases are more complex than in pure Fe(III)-SO_4 systems (Cheng and Demopoulos, 2004; Fleming, 2009; Fleuriault, 2016) because they depend on several operational parameters such as temperature, acidity, Fe/As ratio, and residence time. For example, Sc is generally formed at temperatures <175 °C but can be extended to 200 °C (via FAsH) if the residence time is short enough (Gomez et al., 2011). Meanwhile, the formation of FAsH and BFAS occurs at ≥175 °C. Formation of Sc and FAsH occurs at a low Fe/As ratio (≤ 1), while BFAS and As-BFS precipitate at higher Fe/ As ratios. The AsO_4 rich-BFAS consists of a single-phase, isotypic with the monoclinic form of BFS and is identical to Type 2 (Swash and Monhemius, 1994) /Phase 3 (Dutrizac and Jambor, 2007). In contrast, the SO_4 rich-BFAS consist of a mixture of monoclinic AsO_4-BFAS and BFS with minor Fe_2O_3 (Gomez et al., 2013). As-BFS undergoes substitution of SO_4 with AsO_4 in the orthorhombic polytype structure of BFS (Gomez et al., 2011, 2013), but only 9.8–10 wt% incorporates (Dutrizac and Jambor, 2007; Paktunc et al., 2013). Beyond this incorporation, the arsenate rich-BFAS with a monoclinic polytype crystal structure precipitates. The BFAS is also described by the $AsO_4 \leftrightarrow SO_4$ solid-solution reflected by the inversely proportional SO_4 content. It has been reported that the AsO_4-rich BFAS (SO_4-rich BFAS) can have AsO_4 and SO_4 variations in content from 39 to 50 wt% (26–33 wt%) and 13–22 wt% (26-31 wt%), respectively. Although a detailed study on what exact compositions of AsO_4/SO_4 are needed for the AsO_4-rich BFAS ↔ SO_4-rich BFAS transition remains. However, the solid-solution substitution is greater in the monoclinic compared to the orthorhombic polytype (Dutrizac and Jambor, 2007). Apart from the Fe(III)-AsO_4-SO_4 phases, pure Fe-containing phases (BFS, jarosites, hematite) may precipitate once excess iron is available.

Formation of these Fe(III)-AsO_4-SO_4 phases in real industrial gold POX residues and/or tailings were first reported by Ugarte and Monhemius (1992) who indicated a Zykaite-like phase formed in a pilot plant. Dutrizac and Jambor (2007) observed a Phase 3 (Type 2 = BFAS) with a solid Fe/As ~1.99 to exists from Campbell Mine Tailings (McCreadie et al., 1998, 2000) were high As concentrates (~ 18.5 wt%) had been processed. Unfortunately at this time, no crystal structure for the BFAS polytypes existed (Gomez et al., 2013; Ventruti et al., 2020) so is unclear which form was observed. In 2010, Gomez and co-workers suggested via ATR-FTIR the presence of BFAS from a pilot plant POX residue (Fe/As ~9) from Barrick's Donlin Creek (Gomez et al., 2010). Finally, Paktunc et al. (2013) reported BFAS (= Type 2 = Phase 3) with a Fe/As ~1.32 to occur in a POX residue of a gold commercial operation via As K-edge EXAFS. Unfortunately in this work, the use of TEM-ED to attempt to solve the crystal structure of BFAS was done but yielded an incorrect structure due to the fact it can only be used to obtain a rough estimate (Li and Sun, 2017) and should be followed by synchrotron XRD determination (Gomez et al., 2013).

However, there still lacks a clear understanding as to when such Fe(III)-AsO_4-SO_4 phases may form from the real POX processing of arsenic containing sulfidic gold ores. Thus far in the literature, the use of lab-based equipment (e.g. small volume 2 L, no additional $O_{2(g)}$ overpressure, lack of final stage flash tanks) has been done. However, solution complexation and precipitation/dissolution reaction mechanisms (kinetics and thermodynamics) during the formation of these phases may also be subject to operational physical and chemical factors (e.g. mixing, K_La-volumetric oxygen transfer coefficient, mass transfer, volumetric mass transfer, and dissolution-reprecipitation of unwanted phases during autoclave cooling periods). All of which may or may not be distinct in real industrial operations.

As such in this study, we decided to investigate the precipitation as well as the chemical and mineralogical characterization of various synthetic Fe(III)-AsO_4-SO_4 precipitates. Thus for the first time in the existing literature of such systems, our work here was done at more typical industrial conditions with the aid of a larger scale autoclave, a flash tank, and additional $O_{2(g)}$ overpressure. The first part of the study was conducted on precipitates generated using synthetic solutions. A similar approach was utilized previously (Dutrizac and Jambor, 2007; Gomez et al., 2011; Swash and Monhemius, 1994) in terms of using synthetic based systems but lacked the use of more typically used industrial conditions and equipment as noted above. This allowed to eliminate the potential interferences and produce pure precipitate for chemical and mineralogical characterization. Batch POX leaching of 5 arsenic-containing sulfidic concentrates from different operational mining sites around the world with varying Fe/As ratios (2.7–199) was also piloted. To date, the piloting of real industrial arsenic-containing sulfide concentrates to systematically compare with an ideal synthetic system is not existent in the literature of this topic. Thus our work herein presents the first of such studies. Hence, detailed solution and solid mineralogical analysis were conducted on these to get a clearer picture of how more complex industrial concentrate samples behave in association to the results obtained in the synthetic system.

2. Materials and methods

2.1. Hydrothermal POX synthesis of synthetic precipitates

Analytical grade $As_2O_5.xH_2O$ (Sigma-Aldrich), $Fe_2(SO_4)_3.xH_2O$ (ACE), and 98% H_2SO_4 (ACE) were used for the synthesis of the selected

phases. The starting solutions of various Fe/As molar ratios were prepared. The solutions were prepared at fixed Fe and H_2SO_4 and varied AsO_4 concentrations. Concentrations of Fe and H_2SO_4 were approximated composition of the slurry (Fe and S content) processed via the pressure leaching of base metal sulphide concentrates. The Fe/As molar ratio studied was from 0.99 to 46.17. A solution with no As added was also prepared as a control sample.

The starting concentrations of the solutions used for precipitation of the various phases are listed in Table S2. Fe and H_2SO_4 concentrations were kept constant at 18.2 g/L (except test-J where the Fe was 6.2 g/L) and around 38 g/L, respectively. Meanwhile, the AsO_4 content was varied between 0.00 and 16.2 g/L. These conditions are typical for the pressure oxidation of refractory gold ores and concentrates and similar to conditions employed by other studies (Dutrizac and Jambor, 2007; Gomez et al., 2011). All solutions were prepared with deionized (DI) water. The experiments were carried out using a 4.46 L solution, except the last 2 tests (I and J) where a 2.40 L solution was used.

Arsenic pentoxide (As_2O_5) was used as the source of AsO_4 to avoid the introduction of alkali ions and the precipitation of jarosite-type compounds. In all cases, the starting solutions were heated to 40 °C and stirred for at least 2 h to ensure the complete dissolution of As_2O_5 in the $Fe_2(SO_4)_3$-H_2SO_4 mixture. The clear solutions with no visible precipitate were subsequently transferred to a 1 or 2 gal (3.78 L or 7.57 L) Parr autoclave, sealed in the reactor, and heated to 205 °C where it was maintained at 205 ± 2 °C for a retention time of 90 min. The heating period was approximately 50 min. During the synthesis tests, the impeller speed was 500 rev/min and 5 bar $O_{2(g)}$ overpressure was added to the reactor vapor space to maintain an oxidative atmosphere. The total operating pressure was 23.40 bar. This type of reaction condition was chosen because it is a typical condition used in the POX leaching of gold refractory ores and/or concentrates (Adams, 2016). After the test was complete, the slurry was flashed from the Parr reactor into a flash drum, collected and pressure filtered. Finally, the precipitates were washed with DI water and air-dried before subsequent test work. Both solution and solids were submitted for chemical analyses. It's worth noting here that our study presents the first work on the synthetic system that uses larger volume autoclaves, and the addition of an $O_{2(g)}$ overpressure to the reactors vapor headspace that may be more similar to real industrial operations and may or may not affect mixing, mass transfer, volumetric mass transfer coefficient and chemical reactions (solution/solid). Other previous studies (Dutrizac and Jambor, 2007; Gomez et al., 2011; Swash and Monhemius, 1994) have mainly used smaller volumes ($\leq$ 2 L) and maintained an oxidizing atmosphere by the air initially sealed. As such may not be so close to those encountered in real industrial autoclaves. Furthermore, our study is the first to use a flash drum at the end so that the precipitated solids may be flashed out at representative reaction temperatures. This is preferred to the cooling down method to avoid the precipitation/dissolution of phases that may or may not occur during the cooling periods (up to 1.5 h) as previously reported on this system (Dutrizac and Jambor, 2007; Gomez et al., 2011; Swash and Monhemius, 1994).

The precipitates were washed 10 times by re-pulping in a wet mass to water ratio of 1:5. The first wash was conducted with an acidic solution with a concentration similar to the acid concentration of the final synthesis solution, the second wash was conducted with pH 2 H_2SO_4 adjusted water and the remaining eight washes were conducted with deionized water. Upon washing of the solids, no significant amounts of Fe and As (127–1.66 mg/L and 128–0.20 mg/L) were leached during our washing cycles and no possible phase transformations under washing can occur as these phases are formed under high temperature and pressure. However, a notable amount of S as SO_4 (18400–7.00 mg/L) was observed to leach after the first wash which steadily decreased per cycle upon washing of the solids. Such leaching of SO_4 we can attribute to residual adsorbed SO_4 to the solids from the existing H_2SO_4 in the system. This is because if such amount of leached SO_4 was tied up with our generated solids, then a comparable amount of Fe and As should have also leached simultaneously but this wasn't the case. The precipitates were air-dried before subsequent test work. In cases where a small amount of precipitate was formed, test precipitates were combined for the downstream test work. When sufficient precipitate was produced, only a single test precipitate was utilized. All synthesis tests were duplicated or triplicated here to ensure the reproducibility of the work presented here and generate a sufficient amount of solids for further analysis.

2.2. Batch POX of Au refractory concentrates

To dissolve carbonate minerals in the samples, all concentrates were pulped to 50 wt% solids with DI water and pre-acidified (with 98% H_2SO_4) to an initial free acid concentration of approximately 5 g/L. After agitating the slurry for 1 h, the pre-acidified slurry was filtered and the cake was washed, air-dried, and submitted for chemical assays. The pre-acidified concentrates were oxidized under conditions specified in Table S3 that are typical of industrial POX autoclaves (Adams, 2016). The pre-acidified concentrates were pulped with DI water to the "autogenous" slurry density, which may be calculated per Eq. (2) (Conway and Gale, 1990):

$$\text{Pulp density } (\%) = \frac{100}{0.3\left[S^{2-}\right] + 0.825} \tag{2}$$

The slurry was transferred to a 1 gal (3.78 L) Parr autoclave, the autoclave sealed and heated to 205 °C while the impeller was stirring slowly at 100 rev/min. After the target temperature was reached, the impeller speed was increased to 500 rev/min and a small amount (11 to 20 g) of acid (98% H_2SO_4) was injected into the autoclave with 700 kPag of oxygen, bringing the initial acid concentration to 5 g/L. The slurry was maintained at 205 °C and 7 bar oxygen partial pressure for 90 min. After the leach, the slurry was "flashed" from the reactor into a flash drum, collected and pressure filtered. The POX residues were washed and air-dried before the subsequent test work. All residues, solutions, and wash waters generated were analyzed for Mg, Al, Si, Ca, Cd, Ti, V, Mn, Fe, Co, Ni, Cu, Zn, As, and Pb. Solids were analyzed for Total S, sulfide S, Mg, Al, Si, Ca, Cd, Ti, V, Mn, Fe, Co, Ni, Cu, Zn, As, and Pb.

2.3. Characterization of samples

All precipitates and solutions generated were analyzed for Fe, Ca and S (in solution) using inductively coupled plasma optical emission spectrometry (ICP-OES) while inductively coupled plasma mass spectrometry (ICP-MS) was used for As. All other elements of interest were analyzed via ICP-OES. Both techniques have a detection limit of 0.01 mg/L in solutions and 10 mg/kg in solids. Total S and Sulphides in solids were analyzed with the LECO combustion technique with a detection limit of 0.01 wt%. The sulfate content was determined via the difference of the total S and sulfide. Solids were further analyzed using Scanning Electron Microscopy Energy Dispersive X-ray Spectroscopy (SEM-EDX), X-ray Diffraction (XRD), ATR-FTIR, and Raman spectroscopy. Polished sections were prepared from the selected samples for analysis on the SEM. A Zeiss EVO MA15 scanning electron microscope was used to identifying the minerals/phases present in the sample. Elemental maps of the samples were produced by using Energy-Dispersive Spectrometry (EDS). Backscattered and elemental maps images were captured to illustrate the textural relationships of the different phases.

Powder XRD was conducted using a Bruker D8 Advance X-Ray Diffractometer with a LYNXEYE detector operated at 35 kV and a current of 40 mA. The diffractometer was equipped with a Co Kα radiation ($\lambda = 1.7889$) X-ray source and scans were collected from 3 to 80° 2θ with a 0.02° 2θ step size and a counting time of 3 s per step. The observed peaks were matched to known minerals/compounds using DIFFRACplus EVA and X'Pert Highscore softwares, the PDF database, and our previous published data (Gomez et al., 2011, 2013). The quantitative phase

analyses (QPA) of all powder patterns were performed utilizing the Rietveld refinement technique using the GSAS software (Larson and Von Dreele, 2004) with the graphic user interface EXPGUI (Toby, 2001). Refined parameters were: shifted Chebyschev function background coefficients, zero-shift error, cell parameters, and pseudo-Voigt function peak shape parameters. The preferential orientation correction was also refined for phyllosilicate phases.

The FTIR spectra of the samples were recorded using a Varian 640-IR FTIR spectrometer with a Miracle single bounce diamond ATR (attenuated total reflectance) cell from PIKE Technologies. The FTIR was operated at a resolution of 4 cm^{-1} in the range of 4000 to 550 cm^{-1} over 200 scans. Following analysis, the spectra were baselined using the Varian Resolutions Pro software and compared with our previously published data (Becze et al., 2009; Gomez et al., 2010, 2011, 2013). Raman microscopy was conducted by a Perkin Elmer Raman microscope operated at 785 nm and 60% of the laser power (350 mW excitation source) at the microscope exit. Spectra over the range 3500–100 cm^{-1} were obtained with the accumulation of 5 exposures and an exposure time of 30 s. Raman spectra were compared with our previously published spectra (Becze et al., 2009; Gomez et al., 2010, 2011, 2013).

3. Results and discussion

3.1. Synthetic precipitates

3.1.1. Hydrothermal synthesis, solution data and chemical analysis of precipitates

Results obtained for the precipitation and solid composition of the generated solids are reported in Tables 1 and 2. Based on the chemical composition of the precipitates and previous characterization of similar products by Dutrizac and Jambor (2007), the different phases likely to have precipitated are namely BFS, As-BFS, BFAS, and FAsH (Table 2). Empirical formulae of precipitates were determined based on As/Fe and S/Fe ratios calculated using chemical analysis, OH was calculated to maintain charge balance, while H_2O was determined by difference.

Some scatter in the data was observed in Table 1. Thus, tests D and E conducted at the same feed solution composition showed different performance in terms of AsO_4 and Fe precipitation. The composition of precipitates formed, however, was similar. This effect was also observed for tests F and G and was reported by Dutrizac and Jambor (2007) for low AsO_4 concentrations and attributed to the formation of different compounds at the same conditions.

3.1.1.1. Iron and arsenic precipitation. The effect of Fe/As molar ratio on Fe and AsO_4 precipitation was investigated. Mass of precipitate formed after 90 min of heating in the autoclave at 205 °C was calculated per liter of the solution treated. This allows the comparison of results from tests done in 1 and 2-gal (3.78 L and 7.57 L) vessel and results reported by Dutrizac and Jambor (2007) for 1 L solution. Results are reported in Fig. S1 and Table 1. At conditions tested, Fe precipitation was reported for test A where no AsO_4 was added. We can observe that as the AsO_4 concentration in the feed increased from 0 to 3.28 g/L, the mass of precipitate formed decreased initially reaching a minimum value of around 6.3 g/L solids formed. Then, the mass of precipitate increased again as the AsO_4 concentration in the feed solution increased.

Precipitation results reported by Dutrizac and Jambor (2007) under similar conditions showed the same trend. However, masses of precipitates obtained at $AsO_4 < 2.7$ g/L were lower in their study and could be attributed to longer residence time (3 h vs 1.5 h) and dissolution of some metastable Fe-As compounds initially formed.

The As rejection during the hydrothermal synthesis is an important parameter in view of the desire to fixate all AsO_4 entering the autoclave as a possible stable Fe-As precipitate. The Fe and AsO_4 precipitated, as a percentage of the amount introduced into the feed solution, are shown in Fig. 1 and Table 1. Data obtained in the current study indicated that with increasing Fe/As ratio, both Fe and AsO_4 precipitation passed through a minimum at a value of about 15. The amount of iron precipitated, in general, was lower than that of arsenic. It can be attributed to the high Fe/As ratios used in this study, up to 46. At this condition, iron was partially combined with arsenate to form various mineral phases while the rest remained in solution.

Precipitation results reported by Dutrizac and Jambor (2007) under similar solution concentrations were different from data discussed above with the biggest discrepancy at Fe/AsO_4 ratio above 15 where low AsO_4 and Fe rejections were reported by these authors. This discrepancy could again be attributed to the difference in residence times.

Iron and arsenic precipitation behavior was further analyzed in terms of precipitated Fe/As molar ratio. According to Fig. S2, with an increase of Fe/As ratio in the initial solution (Fe/As_{sol}), the precipitated Fe/As ratio (Fe/As_{ppt}) increased but not linearly. At $Fe/As_{sol} < 20$, similar values for Fe/As in solution and precipitated Fe/As were reported, thus indicating a comparative Fe and AsO_4 precipitation. However, a further increase of Fe/As_{sol} resulted in lower ratio of Fe/As_{ppt} (~ 23 and 46) reflecting changes in the amount of arsenate contained in solid phases formed.

3.1.1.2. Acid generation. The precipitation of iron/arsenate compounds observed was associated with acid generation as reported in Table 1. Final H_2SO_4 concentration in the solution varied between ~47 and 66 g/L while the initial H_2SO_4 concentration was around 38 g/L, indicating that the reactions and generation of the various Fe-AsO_4-SO_4 phases were acid-generating. This result is in agreement with our previous work (Gomez et al., 2008, 2011). The molar ratio of H_2SO_4 generated per AsO_4 was calculated. In general, it was found that the H_2SO_{4gen}/As_{ppt} was in direct correlation with Fe/AsO_4 in the feed (Fig. S3 and Table 1), hence indicating that the acid generated was directly correlated with AsO_4 precipitation even at the larger volume scales used in this work. Noteworthy is the fact that for tests D and E, lower H_2SO_{4gen}/As_{ppt} versus

Table 1
Precipitation results.

Test	Feed solution, g/L			Fe/As molar ratio in feed	Final solution, g/L			Mass of precipitate, g/L solution	Precipitation efficiency[a], %		Molar ratio H_2SO_4 (gen)/AsO_4 (ppt)
	AsO_4	Fe	H_2SO_4		AsO_4	Fe	H_2SO_4		AsO_4	Fe	
A	0.00	18.23	38.02	n/a	0.01	4.11	60.95	41.03	n/a	77.07	n/a
B	0.98	18.23	37.89	46.17	0.02	4.16	61.54	39.19	88.67	75.75	42.78
C	1.97	18.22	37.81	23.06	0.19	9.34	66.45	26.40	81.28	49.10	18.93
D	2.83	18.24	37.97	16.02	0.88	14.76	53.16	16.72	66.94	25.18	9.02
E	2.83	18.24	38.12	16.02	1.45	17.20	49.86	9.75	45.13	11.35	10.04
F	3.28	18.25	37.97	13.84	1.39	15.59	49.85	9.74	48.39	17.18	13.39
G	3.28	18.25	38.00	13.83	1.73	16.88	46.64	6.28	36.96	8.69	12.91
H	3.93	18.25	38.04	11.56	2.04	15.29	52.31	13.12	50.53	22.93	12.01
I	16.14	18.47	38.63	2.85	4.27	7.11	55.34	21.81	55.51	46.95	6.31
J	15.56	6.17	37.31	0.99	1.69	0.81	53.68	16.28	77.41	80.15	2.09

Note: a. precipitation efficiency is the average value calculated using the solution and precipitate analysis.

Table 2
Composition of synthesized precipitates.

Precipitate name	Precipitate composition			AsO_4 /Fe	SO_4/Fe	Fe/AsO_4	Fe/(AsO_4 + SO_4)	Likely phase	Stoichiometric formula
	AsO_4	Fe	SO_4						
	wt%			molar ratio					
A	0.00	33.45	59.76	–	1.04	–	0.96	BFS	$Fe(SO_4)_{1.04}(OH)_{0.92}$
B	1.99	34.10	55.72	0.02	0.95	42.60	1.03	As-BFS	$Fe(AsO_4)_{0.02}(SO_4)_{0.95}(OH)_{1.03}$
C	5.51	32.55	50.93	0.07	0.91	14.69	1.02		$Fe(AsO_4)_{0.07}(SO_4)_{0.91}(OH)_{0.98\ 0.13}\ H_2O$
D	10.85	31.20	52.42	0.14	0.98	7.16	0.90	SO_4-BFAS	$Fe(AsO_4)_{0.14}(SO_4)_{0.98}(OH)_{0.63}$
E	12.03	31.10	50.63	0.16	0.95	6.43	0.91		$Fe(AsO_4)_{0.16}(SO_4)_{0.95}(OH)_{0.64}\ 0.02H_2O$
F	12.68	31.20	43.14	0.16	0.80	6.12	1.03		$Fe(AsO_4)_{0.16}(SO_4)_{0.80}(OH)_{0.90}\ 0.44H_2O$
G	14.19	31.80	43.89	0.18	0.80	5.57	1.02		$Fe(AsO_4)_{0.18}(SO_4)_{0.80}(OH)_{0.86}\ 0.18H_2O$
H	15.12	32.23	40.97	0.19	0.74	5.30	1.08		$Fe(AsO_4)_{0.19}\ (SO_4)_{0.74}(OH)_{0.96}\ 0.22H_2O$
I	27.01	26.27	22.35	0.41	0.49	2.42	1.10	AsO_4-BFAS	$Fe(AsO_4)_{0.41}(SO_4)_{0.49}(OH)_{0.77}\ 2.15H_2O$
J	61.68	27.30	0.87	0.91	0.02	1.10	1.08	FAsH	$Fe(AsO_4)_{0.91}(SO_4)_{0.02}\ 0.93H_2O$

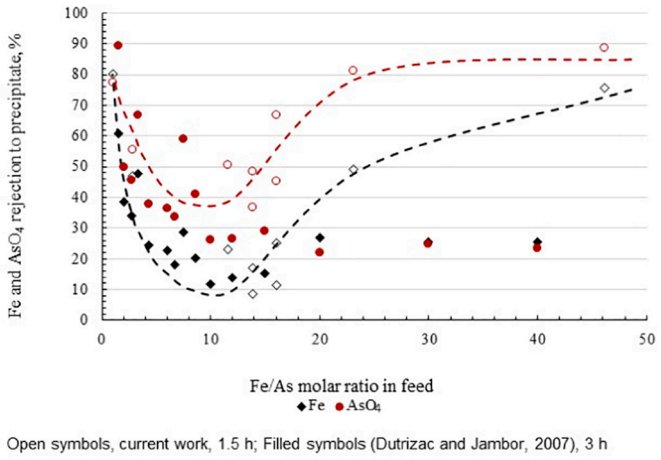

Fig. 1. Fe and AsO_4 precipitation as a percentage of the feed vs. Fe/As ratio in the feed solution.

the Fe/As molar ratio in feed was observed and is likely because more SO_4 was tied up in the solid phase (Table 2). Acid generation per mol of AsO_4 precipitated was investigated in our previous work (Gomez et al., 2011) but only for FAsH and BFAS formed at initial Fe/As ratios from 0.7 to 4, and as such our work here expands this range to what may be more realistically found in the processing of real refractory gold ores and/or concentrates.

3.1.1.3. Chemical composition. The chemical composition and formulae of all precipitates generated during hydrothermal precipitation is reported in Table 2 and and their corresponding experimental conditions can be found in Table 1. The composition of the possible phases identified in our work compared to the data reported previously can be found in Table S4.

BFS. The composition obtained in tests A was similar to the BFS reported by Dutrizac and Jambor (2007) and the theoretical composition of BFS. The empirical formula of BFS determined in this work was $Fe(SO_4)_{1.04}(OH)_{0.92}$ and is close to its ideal formula.

As-BFS. In our work it was found that As-BFS was precipitated when the initial feed molar ratio ranged from 23.1 ≤ Fe/As ≤46.2 (tests B and C). Our solids composition was similar to that reported by Gomez et al. (2011) for a arsenate containing BFS with an initial Fe/As = 12, and the BFS compound incorporating up to 9.8 wt% AsO_4 reported by Dutrizac and Jambor (2007) with Fe/As = 15.

Empirical formulae determined for our As-BFS were $Fe(AsO_4)_{0.02}(SO_4)_{0.95}(OH)_{1.03}$ and $Fe(AsO_4)_{0.07}(SO_4)_{0.91}(OH)_{0.98}0.13H_2O$ which are comparable with the formula derived by Dutrizac and Jambor (2007) [$Fe(AsO_4)_x(SO_4)_x(OH)_z$ were $0 < x \leq 0.12$, $0.91 \leq y \leq 1.02$ and $0.80 \leq z \leq 1.02$].

BFAS. In tests D to I at initial molar feed ratios of 2.9 ≤ Fe/As ≤16.0 basic ferric arsenate sulphate (BFAS) was precipitated. Unlike other types of precipitates identified, BFAS composition ranges were much wider. Fe content in the products was 26 to 32 wt% but arsenate and sulphate contents varied in connection to each other. We can observe that as the Fe/As ratio in the feed solution increased, the amount of arsenate in the solids formed decreased from 27.0 to 10.8 wt% and the amount of sulphate correspondingly increased from 22.3 to 52.4 wt%. Such variations in $AsO_4 \leftrightarrow SO_4$ are typical of the BFAS polytype as we have previously described (Gomez et al., 2010, 2011). Our BFAS phase generated herein is identical to the Type II, Phase 3, and BFAS described previously (Dutrizac and Jambor, 2007; Gomez et al., 2011; Swash and Monhemius, 1994).

Both existing BFAS polytypes, firstly described as Type II + BFS and Type II (Swash and Monhemius, 1994) or Phase 3 + BFS and Phase 3 by Dutrizac and Jambor (2007) and then defined by Gomez et al. (2010, 2013) as arsenate and sulphate rich BFAS were identified in the current study. Noteworthy is the fact that tests conducted at the Imperial College or McGill's Hydrometallurgical labs did not include the initial addition of H_2SO_4. Herein, AsO_4-BFAS was precipitated at an initial Fe/As feed ratio of 2.85 (test I) while SO_4-BFAS was formed at higher Fe/As ratios of 11.6 ≤ Fe/As ≤16.0 (tests D to H). In comparison, Dutrizac and Jambor (2007) reported precipitation of pure Phase 3 (AsO_4-BFAS) at similar test conditions and 2.7 ≤ Fe/As ≤3.3, while the mixture Phase 3 + BFS (now referred to as SO_4-BFAS) was formed at 4.3 ≤ Fe/As ≤12.0.

Our Basic ferric arsenate sulphate produced had formula $Fe(AsO_4)_x(SO_4)_y(OH)_z{\cdot}wH_2O$ where $0.14 \leq x \leq 0.41$, $0.49 \leq y \leq 0.98$, $0.63 \leq z \leq 0.96$ and $0 \leq w \leq 2.15$. There is a similarity between the empirical formulas obtained in this study and the generic formula for BFAS $Fe(AsO_4)_{1-x}(SO_4)_x(OH)_x\bullet\ (1\text{-}x)H_2O$ with $0.3 < x < 0.7$ proposed in our previous work (Gomez et al., 2011). Data presented here are also in line with Dutrizac and Jambor's (2007) generalized formula of their Phase 3 that is $Fe[(AsO_4)(SO_4)]_{\sum 1}(OH, H_2O)_{\sum 1}$ and the compositional range from $Fe(AsO_4)_{0.25}(SO_4)_{0.75}(OH)_{0.75}$ to $Fe(AsO_4)_{0.54}(SO_4)_{0.46}(OH)_{0.36}$.

The current study also allowed to differentiate the composition of the SO_4-rich BFAS from AsO_4-rich BFAS while having the same general formula $Fe(AsO_4)_x(SO_4)_y(OH)_z{\cdot}wH_2O$. In the case of SO_4-BFAS, it had a composition of $0.14 \leq x \leq 0.19$, $0.74 \leq y \leq 0.98$, $0.63 \leq z \leq 0.96$ and $0 \leq w \leq 0.44$ while the AsO_4-BFAS had higher x = 0.41, lower y = 0.49, z = 0.77 and w = 2.15.

FAsH. In test J, at a initial molar feed of Fe/As = 1.0, the ferric arsenate sub-hydrate (FAsH) product was formed whose composition corresponded well with that of FAsH, Type I, and Phase 4 reported previously (Dutrizac and Jambor, 2007; Gomez et al., 2011; Swash

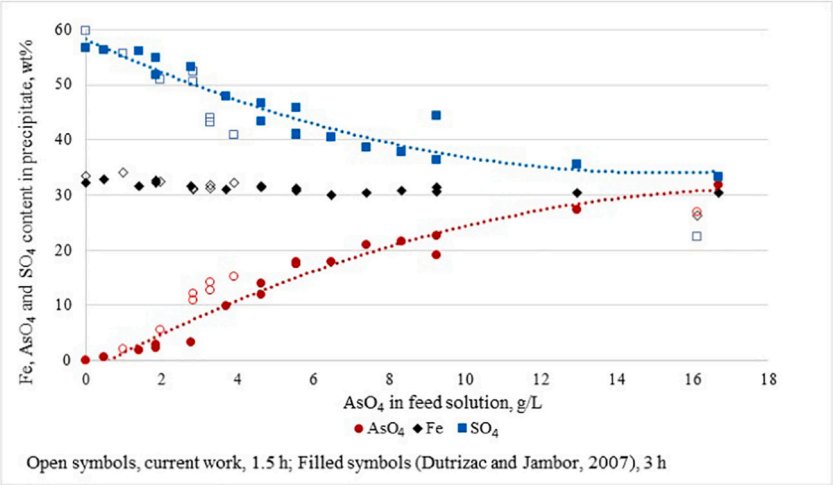

Fig. 2. Precipitate composition vs. AsO_4 addition in the feed solution.

and Monhemius, 1994). The empirical formula determined for our FAsH was $Fe(AsO_4)_{0.91}(SO_4)_{0.02}0.93H_2O$ which contains slightly larger amounts of water than previously reported but this is because it was not accurately measured via TGA but rather from the difference. By comparison, formulae derived previously were $FeAsO_4 \bullet wH_2O$ with w = 0.54 reported by Dutrizac and Jambor (2007) and w = 0.72 by Gomez et al. (2011).

The composition of all precipitates A to I, as a function of AsO_4 addition in the feed, is graphically shown in Fig. 2. The Fe content was similar, ranging between 26.3 and 34.1 wt%. However, an inverse relationship, evident of substitution between the AsO_4-group and the SO_4-group, was observed. This relationship was also previously noted by Dutrizac and Jambor (2007). The data published from their studies, which confirmed this trend, is included in Fig. 2. It is noted that the precipitates produced by Dutrizac and Jambor (2007) contained slightly less arsenate and more sulphate compared to the precipitates produced during the current work. A possible reason for this is the difference in retention time (i.e., 1.5 h vs. 3 h). According to observations done by Dutrizac and Jambor (2007), the ratio of arsenate to sulphate in the precipitate is a function of retention time, and increased contact with the synthesis solution will result in the gradual displacement of arsenate by sulphate which can also be observed spectroscopically (Gomez et al., 2008).

3.1.2. *Mineralogical characterization*

Six of the ten precipitates in Table 2 were selected for SEM-EDX analysis. These precipitates were most likely to represent the BFS, As-BFS, BFAS and FAsH phases from previous works based on their bulk chemical compositions (Dutrizac and Jambor, 2007; Gomez et al., 2011; Swash and Monhemius, 1994). The images of these precipitates are shown in Fig. S4. All precipitated particles, except for precipitate J, had similar sizes of about 10 μm to 70 μm. The precipitated BFS with no As showed nucleation and growth processes where dendritic growth was common. Its point analysis chemical composition was close to that found in the bulk (Table 2) and expected for the BFS phase (Fleming, 2009; Gunaratnam et al., 2018). The particles with lower AsO_4 content ($\leq$ 5.5 wt% AsO_4) had dendrites at the edges of the particles whereas particles with AsO_4 content $\geq$15.1 wt% were smooth at the edges (Fig. S4d). Thus indicating that for the BFS and As-BFS, the particle formation may not have formed under ideal equilibrium development conditions as their growth occurred along more energetically preferred crystallographic directions. This often occurs due to concentration gradients from supersaturated values in solution to the concentrations in equilibrium with the crystals at the surface. This is in contrast to the sulfate-rich BFAS, arsenate-rich BFAS, and FAsH phases where non-dendritic particles were found to precipitate. This may be an indication that when they are nucleated and formed, their growth rate is not only limited by the rate of diffusion of the solute atoms at the interface. And that their concentration gradients from the supersaturated values/regions in solution may be similar to the concentration values/regions in equilibrium with the crystals at the surface. Arsenic was not visible in the elemental maps of Precipitate B and Precipitate C, due to low concentrations, but was detected by EDS on the selected points. It is worth pointing out that both precipitate B and C showed particles that had similar chemical compositions to the bulk results (Table 2) but some particles analyzed showed significantly less concentration of AsO_4. Such differences in the AsO_4 concentration observed for certain particles may arise from the variance in solution concentration gradients from supersaturated regions to those concentrations that exist in equilibrium with the crystal at the surface that leads to dendritic growth. In contrast to the red/orange-colored particles of Precipitates A, B, and C (Fig. S4), a yellow/green color dominated the particles of Precipitate H and I, which clearly showed AsO_4 in both elemental mapping and EDS point analysis. From the EDS analysis of precipitate H and I, we could observe that their chemical compositions were slightly distinct to the observed bulk composition (Table 2) for the predicted AsO_4 and SO_4-rich BFAS phases but followed a similar trend. Furthermore, based on the micro-particle elemental analysis, we could observe that a notable replacement of $SO_4 \leftrightarrow AsO_4$ occurred while the Fe concentration remained fairly similar as previously observed for the BFAS solid solution (Gomez et al., 2010, 2011). Furthermore, it is worth noting that both H and I precipitates displayed point analysis of different particles that were similar in AsO_4 concentration (unlike those of particles B and C) which may again highlight the difference in the way the BFAS phase nucleates and grows vs. that of As-BFS/BFS. Precipitate J, which contained the highest amount of arsenic, appeared to consist of smaller particles vs. other precipitates in this study. Point EDS analysis of Fe and particularly AsO_4 were found to be higher than those found in the bulk analysis (Table 2) and expected for the previously reported FAsH (Dutrizac and Jambor, 2007; Gomez et al., 2011; Swash and Monhemius, 1994). Such differences may be a result of the fact that ICP-OES is more accurate at the bulk scale in comparison to SEM-EDX analysis (Einhauser, 1997) which is more locally sensitive to variations.

The FTIR spectra of Precipitates A to J are displayed in Fig. 3 while the Raman spectra of Precipitates A to I are shown in Fig. S5 and suggested vibrational assignments are presented in Tables S5–S6. The SO_4 and AsO_4 bands are indicated on these plots. The theoretically published spectra for the SO_4-BFAS, AsO_4-BFAS, As-BFS, FAsH, scorodite, and jarosite were also included for comparison purposes. The suggested

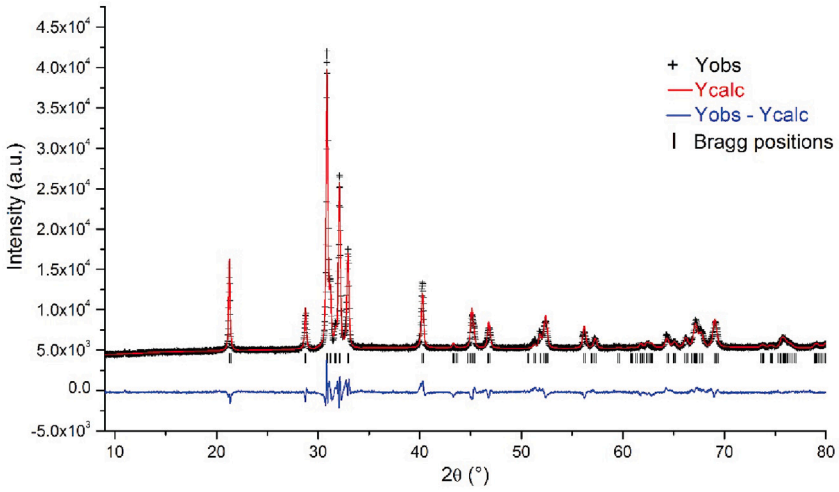

Fig. 3. Comparison of FTIR-IR spectra of synthesized precipitates.

vibrational assignments for these may be found in our previous works (Gomez et al., 2010, 2011, 2013; Becze et al., 2009). It should be noted that at low AsO_4 content (≤2 wt% - sample B), our experimental data and the theoretical published FTIR and Raman As-BFS spectra matched only that of BFS (Gomez et al., 2013; Powers et al., 1975). This is because such lab-based techniques are not sensitive enough to detect such low molecular concentrations. However, for the 5.5 wt% AsO_4 sample C, the characteristic ν_3 (AsO_4) IR active band at ~850 cm^{-1} and the corresponding Raman band were observed. As seen on both FTIR and Raman plots, with an increase in precipitate AsO_4 content, the AsO_4 vibrational band strength increased. On the one extreme, the FTIR and Raman spectra of Precipitate A-C which contained 0–5.5 wt% AsO_4, largely matched our standard and published spectra for As-BFS (Gomez et al., 2013). The Raman and FTIR spectra of Precipitate D–H with 10.8–15.1 wt% AsO_4 correlated with that of the standard and our published SO_4-BFAS (Gomez et al., 2013). Precipitate I with the AsO_4 content of 27.0 wt% had an FTIR spectrum which is difficult to identify as it has bands corresponding to both the SO_4-BFAS and AsO_4-BFAS (Gomez et al., 2013). However, its Raman (Fig. S5) indicated that the sample is AsO_4-BFAS. This fact confirmed that the AsO_4-BFAS phase exists at a wider AsO_4 solid content range than it was previously reported (Gomez et al., 2010). The spectra of Precipitate J which contained 61.7 wt% AsO_4, matched well the theoretical FAsH (Gomez et al., 2011) and not Sc as expected for such high temperature used in the POX processing of gold concentrates and ores. A high correlation between published and measured spectra, therefore, confirms the nature of the precipitates produced at the two extremes. Meanwhile, precipitates with intermediate compositions therefore likely consist of SO_4-rich BFAS and AsO_4-rich BFAS along with As-BFS. Thus indicating that the larger volume used for the autoclave, the addition of $O_{2\ (g)}$ overpressure, initially added H_2SO_4 and the use of flash drum at the end to avoid dissolution/reprecipitation of unwanted phases did not significantly affect the products formed in comparison to previous works (Dutrizac and Jambor, 2007; Gomez et al., 2011; Swash and Monhemius, 1994). However, our precipitates formed herein may be more representative of precipitates that can be found in autoclave residues after the pressure oxidative treatment of auriferous arsenical concentrates versus previous studies.

The XRD diffractograms for Precipitates A to H in comparison to our reference standards are presented in Fig. S6. It is worth noting that BFS, As-BFS, and the BFAS solid solution essentially belong to the family of OD polytypes where the orthorhombic and monoclinic are the most favorable but the monoclinic has a slightly greater activation energy of formation (Gomez et al., 2013; Ventruti et al., 2005). In the case of the BFAS solid solution, the AsO_4-rich BFAS variety favors the monoclinic while the SO_4-rich BFAS is a mixture of the former, and monoclinic BFS and hematite. Therefore, based on our XRD work (Fig. S6), the exact phase (i.e. As-BFS, BFS, SO_4, or AsO_4-rich BFAs) generated for samples A-H couldn't be assigned without a doubt due to the high similarity of the diffractograms that arises from the fact they belong to this family of OD structures. This is in agreement with previous reports (Dutrizac and Jambor, 2007; Gomez et al., 2011) without the use of synchrotron-based XRD and crystallographic modeling (Gomez et al., 2013; Ventruti et al., 2005) to further verify structural results. However, based on the chemical, vibrational, and XRD data as well as previous works, we can indicate that samples A belongs to BFS, samples B–C belong to As-BFS and D–H are in the form of the SO_4-rich BFAS. To further verify the identity of our sample with the second-highest amount of AsO_4 (27%, I), additional Rietveld refinement was conducted (Fig. 4 and Table S7). This showed that sample I was indeed composed of a single monoclinic phase (Ventruti et al., 2020) the AsO_4-rich BFAS, in agreement with our vibrational analysis and previous reports (Gomez et al., 2011, 2013). Finally, in the case of sample J with the highest amount of AsO_4, Rietveld refinement (Fig. 4 and Table S7) showed it to belong to the FAsH phase (≤1.5% Sc), in agreement with the chemical and vibrational analysis.

3.2. Real concentrates and ores

3.2.1. Chemical characterization of concentrates

Five sulphide concentrates were sourced from various operational gold mines around the world and whose chemical composition is shown in Table S8. The As content varied between 0.2 and 8.3 wt%, while the Fe content varied between 8.9 and 24.3 wt%. Consequently, the molar ratio between Fe and As ranged between 2.7 and 199.5. The sulphide content constituted the majority of the total sulfur present as expected in the range between 8.2 and 33.8 wt%. Other impurity elements included Sb, Si, K, Na, Mg, Al, and Ca.

3.2.2. Mineralogical characterization of concentrates

The mineralogical composition of the concentrates determined via XRD is included in Table S9. All concentrates contained pyrite as the main sulphide bearing mineral, ranging between 12 and 52 wt%. Apart from pyrite, samples #2 and #3 also contained pyrrhotite as an iron-sulphide mineral, ranging in content between 10 and 25 wt%. The main source of As is arsenopyrite which ranged between 1 and 15%, with the highest content found in sample #5 and lowest sample #1, leading to the respective Fe/As molar ratios (Table S8). Although not a focus of this work, the primary source of Sb was stibnite (Sb_2S_3) which was present in four of the five concentrates in varying proportions ranging between 1.4 and 3.8 wt%.

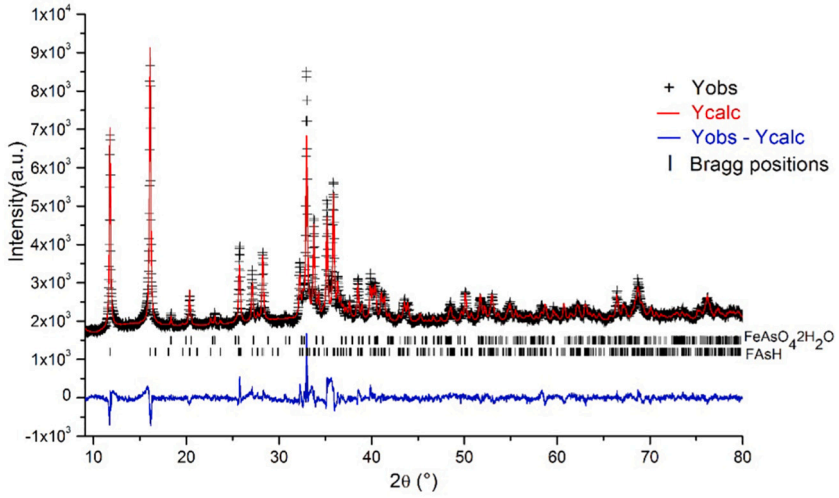

Fig. 4. XRD diffractograms showing Rietveld refinement for Precipitate I and J.

Table 3
Batch POX solution tenors.

Sample #	Al	AsO_4	Ca	Fe	K	Na	Mg	Si	Sb	Fe^{2+}	Fe^{3+}	Fe/As molar ratio	H_2SO_4	Slurry density
	mg/L												g/L	%
#1	991	61	39	5790	70	38	21	645	0	204	5586	235.4	60	9
#2	1320	1686	438	7210	50	40	2440	652	1	288	6922	12.9	45	21
#3	789	1640	862	8405	347	55	261	913	5	264	8141	12.7	52	15
#4	1620	1993	933	5830	147	107	475	793	2	264	5566	7.2	54	29
#5	1600	1552	544	4790	54	25	651	647	0	168	3980	7.6	35	15[b]

Note: b. Test not conducted at autothermal slurry density due to sample limitations; slurry cooled i.e., not flashed.

3.2.3. Batch POX

The concentrates were submitted to batch POX testing as outlined in Section 2.2. As may be observed from Table 3, batch tests were conducted at different slurry densities based on the sulphide content in the concentrates (see Eq. (2)). This was done for all concentrates except for the test conducted on concentrate #5 which had been done at 15 wt% instead of the autogenous slurry density of ~20 wt% due to sampling limitations. The composition of the batch POX solutions and free acid concentrations after oxidation are presented in Table 3.

Based on Table 3, we can observe that relatively high levels of soluble Fe remain in all POX solutions (4.1–8.4 g/L). It has been reported (Fleuriault, 2016) that in general, more Fe remains in solution after POX when BFS forms vs. hematite since the former has a lower solid Fe concentration. Moreover, BFS solubility's under hydrothermal conditions is greater than hematite. Similarly, the precipitation of SO_4-BFAS has been documented (Gomez et al., 2011) to have lower Fe precipitation efficiencies (53–79%) as the Fe/As molar ratio increases. In contrast, the AsO_4-rich BFAS has higher Fe precipitation efficiencies of 76–88%. In our case, the amount of Fe precipitated in the POX residue (Table 4) relevant to the initial sulphide concentrate content was ≥86%, thus been similar to those previously observed for the BFAS system (Gomez et al., 2011). The remaining AsO_4 in solution after POX processing of the concentrates ranged between 0.06 and 1.99 g/L, while the AsO_4 precipitation efficiencies of the POX residues (relative to the initial sulphide concentrates) were observed between 88 and 100%. Thus indicating that the majority of AsO_4 was removed into the solid phase (i.e. POX residue) as desired (Fig. S7). Comparison of the possibly generated synthetic phases in our work (Table 2) and our previous works (Gomez et al., 2011) indicate that the observed precipitation efficiencies in the POX concentrate lie in the range of As-BFS and the BFAS polymorphs. In general, the AsO_4 rejection reported for concentrate samples was high (88–100%). Both, Fe and AsO_4 rejection was however higher than values reported for synthetic precipitates (Table 1) generated at a similar Fe/As ratio in the feed. The difference in the behavior of the synthetic studied system and actual samples could be due to (1) complex mineralization of actual samples and presence of Fe and (2) As in different mineral phases such as arsenopyrite, pyrite, and pyrrhotite which have different oxidation kinetics during pressure oxidation. Therefore, the dissolution-precipitation ratio of soluble Fe/As in the POX reactor is different from the observed ratio of the total amount of elements. Furthermore, the presence of Al, K, Mg, and Na in the sulphide concentrates could also potentially promote the formation of jarosite-alunite phases in the POX residues.

The free acid levels in the POX solutions ranged between 35 and 60

Table 4
Batch POX solid residue composition.

Sample #	Al	As	Ca	Fe	K	Na	Mg	Si	Sb	S^{2-}	Total S	SO_4	Fe/As molar ratio
	wt%												
#1	3.3	0.2	0.1	22.9	0.6	0.1	0.1	9.5	0.0	0.03	12.1	36.2	153.6
#2	2.4	2.6	0.7	17.5	0.4	0.2	6.2	20.6	0.0	0.11	3.5	10.1	9.0
#3	1.4	6.4	2.3	22.5	0.3	0.1	0.1	10.0	6.6	0.10	4.5	13.1	4.7
#4	7	4.5	0.2	10.3	1.3	2.8	0.3	24.1	0.8	0.13	2.4	6.7	3.1
#5	5.1	8.2	0.2	14.4	1.5	0.1	0.2	17.4	3.5	0.03	1.8	5.2	2.4

g/L (Table 3). Assuming an initial free acid concentration of 5 g/L, we observed that all concentrates generated ~30–55 g/L net free acid. Based on synthetic previous works (Fleming, 2009; Fleuriault, 2016), it was assumed that the formation of BFS (and jarosites) is favored at >20 g/L initial free acidity, > 40 g/L final free acidities while a net increase of ~ ≥ 41 g/L marks the limit for its formation. Below these initial/final free acidities or net increases ≥41 g/L, hematite formation dominates. Reasons for this lie in the fact that hematite is normally associated with greater production of H_2SO_4 while BFS consumes it, thus this is why we may expect high acidities to promote BFS formation. However, BFS has been proven in some cases to form even when hematite would yield favorably, especially under real processing conditions where solution chemistry and mineralization are complex. Thus in concentrate samples that have final free acidities of ≥40 g/L, we may expect to have BFS (and/or jarosites) precipitate but to be further verified by XRD. Interestingly, sample # 2 with a final free acidity of 45 g/L and a net increase of ~40 g/L lies in the middle of the theoretical BFS-hematite synthetic acidity boundary and as such we may infer it to have some hematite formation. Moreover, filtrate produced during leaching of sample #2 had 2.44 g/L Mg and according to the finding from Sasaki et al. (1994) buffering effect of Mg may lead to increasing stability region at which hematite forms. The formation of BFAS is acid generating (Gomez et al., 2011), where its precipitations makes ~2 mol of H_2SO_4/mol of As precipitated or 1 mol of H_2SO_4/mol of Fe precipitated. Furthermore, based on available data, the AsO_4-rich BFAS is associated with a greater final and generated free acidity versus that of the SO_4-rich BFAS (a mixture of AsO_4-rich BFAS, BFS, and hematite). These free acidities for the BFAS polytypes (Gomez et al., 2011) tend to be lower than those observed for the BFS system and as such we may expect to have the formation of the BFAS polytypes in the majority of the concentrate samples studies, except for sample #1 who had the largest free acidity.

As can be observed in Table S10, near-complete sulphide oxidation was achieved during all tests as the sulphide content was ≤0.70 wt% in the residues. Hence, indicating that the selected batch-test conditions were appropriate to fully leach the gold from its refractory matrix (Adams, 2016). It is interesting to note that the Fe/As molar ratios obtained in the batch POX residues (Table 4) were 2.4–153.6 and roughly corresponded to the same ratios observed in the initial sulphide concentrate feed (Table S8) of 2.7–199.5. Thus further indicating that the operational parameters chosen in our study to leach the sulphide concentrates were efficient in the removal and entrapment of Fe and AsO_4 in the solid residue phase. The presence of sulphate in the POX solid residue (Table 4) was highest in sample #1 (36.2 wt%), and lowest in sample #5 (5.2 wt%), thus indicating the possible existence of sulphate based phases (e.g. BFS, As-BFS, BFAS polytypes and/or jarosites). However, further mineralogical characterization is needed and are discussed in the following section.

3.2.4. Mineralogical characterization of POX residues

The mineralogical phase composition as determined by XRD of the POX residues is included in Table S10. Based on this analysis, we observed that the majority of Fe and As precipitated as Fe-As hydroxy sulphates (i.e., BFAS or As-BFS and BFS). In terms of Fe-containing phases which may or may not contain AsO_4, jarosite, BFS, and iron oxides were detected. Notable amounts of jarosite phases were found in samples # 1 to 5 while residue #2 contained noticeable amounts of hematite.

It is worth noting that even though residues #3 and 5 contained a significant amount of Sb (3.5–6.8 wt%), Sb-bearing phases were not detected in the residues (Table S10). Thus indicating that Sb-containing POX precipitates were not identified by the DIFFRACplus EVA nor X'Pert Highscore softwares based on the built-in database of known compounds. Thus additional refinement of published diffractograms of Sb-oxides and possibly Sb-Fe-SO_4 phases not in the databases against the measured XRD diffractogram will have to be done in the future but for now, it is out of the scope of this study.

To further compare the POX residues in terms of As and Fe deportment, the various Fe and As phases found in this work were normalized to the sum of all Fe-AsO_4-SO_4 phases in each POX residue (Fig. 5). As expected, when the Fe/As ratio in the sulfide feed and final POX residue was high (sample #1), As-BFS/BFS was formed. However, at a lower Fe/As ratio in the industrial samples (feed and residue), As precipitated as BFAS in the POX residue. This trend observed for the industrial samples is in agreement with what we observed in our generated synthetic samples (Section 3.1) and previous literature works (Dutrizac and Jambor, 2007; Gomez et al., 2011, 2013; Swash and Monhemius, 1994).

The FTIR (Fig. 6) of the generated POX residues was further collected to verify the possible Fe(III)-AsO_4-SO_4 phases detected via XRD. Suggested vibrational assignments can be found in Table S11. In general, all samples exhibited strong $\nu_{1,3}$ (SO_4) modes between ~950 and 1250 cm^{-1} that were found to split in degeneracy as expected for BFS, BFAS, and jarosite type of phases (Gomez et al., 2010; Powers et al., 1975; Spratt et al., 2013). In contrast, the definitive $\nu_{1,3}$ (AsO_4) modes between 700 cm^{-1} to below 950 cm^{-1} as observed for BFAS phases (Gomez et al., 2013) were only clearly observed for samples # 3 and #5. As expected, sample #1 resembled only that of As-BFS/BFS meanwhile samples #2 and #4 also showed this signature but its $\nu_{1,3}$ (SO_4) modes appeared to be mixed with symmetry also generated by the BFAS polytypes. It is worth noting that for sample #4, its FTIR spectra largely resembled that of Albite (McKeown, 2005), in agreement with our XRD phase analysis. In this case, the $\nu_{1,3}$ (AsO_4) modes of samples #2 and 4 were not clearly defined to be able to separate if they occurred in the specific type of group symmetry as observed for the BFAS polytypes (Gomez et al., 2010, 2013). For sample #3, the $\nu_{1,3}$ (SO_4) region also exhibited a mixed vibrational band symmetry between that of the As-BFS/BFS and the BFAS polytypes. However, the $\nu_{1,3}$ (AsO_4) modes between 750 and 850 cm^{-1} were typical of those observed for the BFAS polytypes (Gomez et al., 2010, 2011, 2013) thus supporting the XRD findings. It is worth noting that the incorporation of AsO_4 into the BFS or jarosite structures (≤ 9.8–10 wt%) does not evidently break the degeneracy of the ν_3

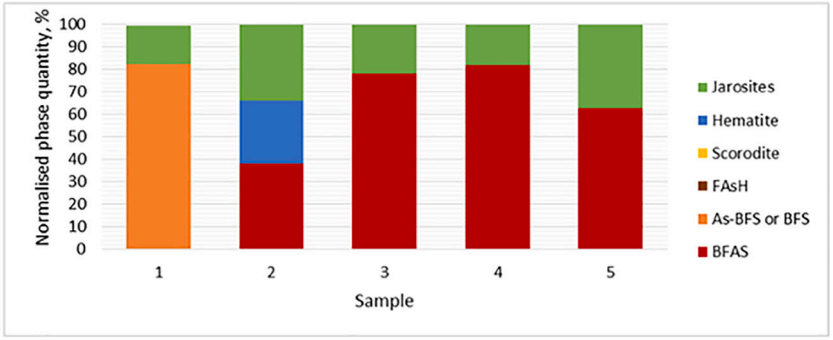

Fig. 5. Normalized phase contribution Fe-As phases in POX residues.

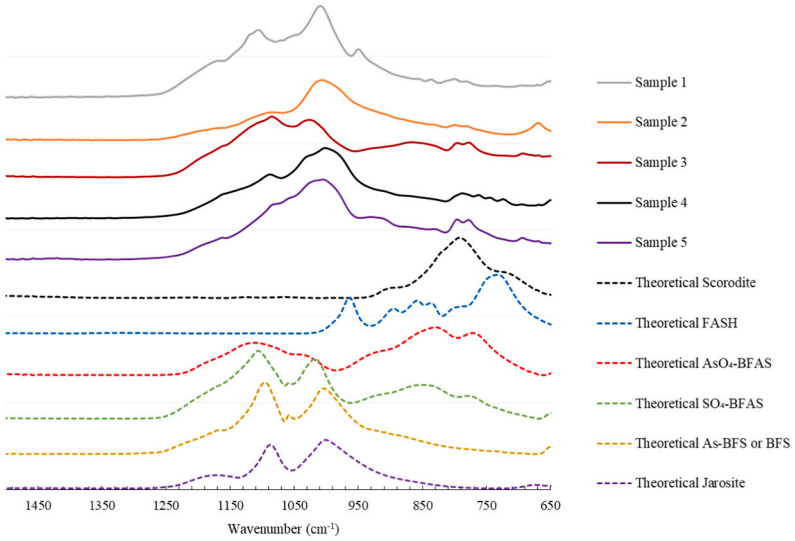

Fig. 6. FTIR-IR spectra of POX residues.

(AsO_4) IR active mode based on data collected here and literature data (Aguilar-Carillo et al., 2018; Dutrizac and Jambor, 2007; Gomez et al., 2013; Paktunc and Dutrizac, 2003; Powers et al., 1975; Reyes et al., 2017; Savage et al., 2003). This is in contrast to the BFAS polytypes for which the degeneracy of the ν_3 (AsO_4) IR active mode is broken (Gomez et al., 2010, 2013). It is worth mentioning that SiO_2 is an inherent part of the POX residues and generates SiO_4 bands at 694, 778, and 794 cm^{-1} (Madejova et al., 2017; Ojima, 2003) which may be observed in all samples except for #1. However, for sample #3 (and #5), the ν_3 (AsO_4) band ~830–867 cm^{-1} was observed and the band at ~779 cm^{-1} may also be tentatively assigned to the ν_1 (AsO_4) mode from the BFAS polytypes (Gomez et al., 2010, 2013) since the As content is sufficient enough to detect via ATR-FTIR and is in agreement with the XRD analysis.

4. Conclusions

For the synthetic Fe-As phases produced under larger volumes and conditions more closely to industrial operations, we found that as more H_3AsO_4 was introduced to the $Fe_2(SO_4)_3$-H_2SO_4 mixture, the Fe and As rejection efficiencies decreased. This is unlike our previous synthetic work under different operational parameters (e.g. retention time and initial H_2SO_4) which may affect the precipitation and solubility of the Fe-AsO_4-SO_4 phases. The highest As precipitation efficiency (~ 88%) was observed when As-BFS formed at an initial feed of Fe/As = 46 while a decrease in efficiency (~ 81 to 37%) occurred at Fe/As = 23 to 3 and was accompanied by the precipitation of BFAS. Mineralogical characterizations indicated that BFS, As-BFS, AsO_4/SO_4-rich BFAS, and FAsH were dominant. All reactions generated acid with BFS/As-BFS producing the largest amounts in comparison to all other phases. Finally, the confirmation of the AsO_4-rich BFAS at an initial Fe/As feed of 2.8 expands its formation domain.

Given the synthetic results, POX batch tests on real concentrates with similar feed Fe/As ratios were conducted for comparison. It was found that the solution Fe and As rejection behavior was different than in these synthetic tests but similar to some of our previous work. Thus highlighting that operational parameters (e.g. residence time, initial acidity, and volume) have an impact in comparing ideal synthetic systems and likely arise from the complex dissolution-precipitation that occurs in real concentrate POX. Mineralogical analysis indicated that jarosite, hematite formed but As-BFS/BFS dominated at a high initial Fe/As feed ratio (199) while BFAS precipitated at Fe/As 2.7 to 9.6. Acid generation was common to all tests and similar to these synthetic tests, the greatest amounts produced were associated with the formation of As-BFS/BFS versus all other phases formed.

Declaration of Competing Interest

The authors have no competing interests to declare.

Acknowledgments

The authors thank MINTEK (South Africa) for the support of this work. The following people are also acknowledged: Johanna Mörtberg (Luleå University of Technology, Sweden), Ndamulelo Negota, Christoph Pawlik, Tebogo Gopane, and Zinhle Mabasa. MAG acknowledges the support of Prof. Yongfeng Jia, the National Key R&D Program of China (No.2017 YFD 0800301), and the National Natural Science Foundation of China (No. 41703129). The authors acknowledge Professor George Demopoulos at McGill University for his kind advice and support.

Appendix A. Supplementary data

Supplementary data to this article can be found online at https://doi.org/10.1016/j.hydromet.2021.105616.

References

Adams, M.D., 2016. Gold Ore Processing: Project Development and Operations, Second ed. Elsevier, Amsterdam (ISBN: 978-0-444-63658-4).
Aguilar-Carillo, J., Villa-Lobos, J., Pi-Puig, T., Escobar-Quiroz, I.N., Romero, F.M., 2018. Synergistic arsenic (v) and lead (ii) retention on synthetic jarosite. I simultaneous structural incorporation behaviour and mechanism. Environ. Sci. 20 (2), 354–369.
Becze, L., Gomez, M.A., Le Berre, J.F., Pierre, B., Demopoulos, G.P., 2009. Formation of massive Gunningite-Jarosite scale in an industrial zinc pressure leach autoclave – a characterization study. Can. Metall. Q. 48, 99–108.
Cheng, T., Demopoulos, G.P., 2004. Hydrolysis of ferric sulfate in the presence of zinc sulfate at 200 °C: precipitation kinetics and product characterization. Ind. Eng. Chem. Res. 43 (20), 6299–6308.
Conner-Mills, K., Anderson, C., 2018. Pressure oxidation of enargite concentrates containing gold and silver. In: Davis, B., et al. (Eds.), Extraction 2018, The Minerals, Metals & Materials Series. Springer, pp. 1645–1659. https://doi.org/10.1007/978-319-95022-8. ISBN: 978-3-319-95021-1.
Conway, M.H., Gale, D.C., 1990. Sulfur's impact on the size of pressure oxidation autoclaves. J. Miner. Met. Mater. Soc. 42 (9), 19–22.
Coudert, L., Bondu, R., Rakotonimaro, T.V., Rosa, E., Guittony, M., Neculita, C.M., 2019. Treatment of As-rich mine effluents and produced residues stability: current knowledge and research priorities for gold mining. J. Hazard. Mater. 386 https://doi.org/10.1016/j.jhazmat.2019.121920.

Das, G.K., Archarya, S., Anand, S., Das, R.P., 1996. Jarosites: a review. Min. Process. Extr. Metall. Rev. 26 (3–4), 185–210.
Dutrizac, J.E., 1987. Overview of iron precipitation in hydrometallurgy. In: Strathdee, G. L., Klein, M.O., Melis, L.A. (Eds.), Crystallization and Precipitation. Pergamon Press, New York, pp. 259–283.
Dutrizac, J., Jambor, J., 2007. Characterization of the iron arsenate-sulphate compounds precipitated at elevated temperatures. Hydrometallurgy 86, 147–163.
Einhauser, T.J., 1997. ICP-OES and SEM-EDX analysis of dust and powder produced by the laser processing of a Cr-Ni-steel alloy. Mikrochim. Acta 127, 265–268.
Fernandez, R.R., Collins, A., Marczark, E., 2010. Gold-recovery from high-arsenic-containing ores at Newmont's roasters. Min. Metal. Explor. 27, 60–64.
Filyanin, G.A., Vorobev-Desatovskiy, N.V., 2014. Amursk hydrometallurgical plant is a key element of processing unit of far Eastern "Polymetal". JSC. Tsvetn. Met. 6, 29–36.
Fleming, C., 2009. Basic Iron Sulphate - A Potential Killer for Pressure Oxidation Processing of Refractory Gold Concentrates if Not Handled Appropriately. Technical Bulletin SGS Mineral Services.
Fletcher, B., 2012. Investor Day – Lihir. Investor Day, Sydney. October 02, 2012. http://www.newcrest.com.au/media/presentations/2012/FINAL_Lihir.pdf.
Fleuriault, C., 2016. Iron Phase Control During Pressure Leaching at Elevated Temperature. M.Sc. Colorado School of Mines.
Frostiak, J., Haugard, B., 1992. Start up and operation of Placer Dome's Campbell Mine gold pressure oxidation plant. Min. Eng. 44 (8), 991–993.
Gold Exploration, 2012. Mining Journal Special Publication, pp.62.
Gomez, M., Becze, L., Bluteau, M., Le Berre, J., Cutler, J., Demopoulos, J., 2008. Autoclave precipitation and characterization of Fe(III)-AsO4-SO4 phases. In: Young, C., Taylor, P., Anderson, C., Choi, Y. (Eds.), Hydrometallurgy 2008. Society from Mining, Metallurgy and Exploration, Littleton, p. 1078.
Gomez, M.A., Assaaoudi, H., Becze, L., Cutler, J.N., Demopoulos, G.P., 2010. Vibrational spectroscopy study of hydrothermally produced scorodite (FeAsO4·2H2O), ferric arsenate sub-hydrate (FAsH; FeAsO4·0.75 H2O) and basic ferric arsenate sulphate (BFAS; Fe[(AsO4)1-x(SO4)x(OH)x]·wH2O). J. Raman Spectrosc. 41, 212–221.
Gomez, M., Becze, L., Cutler, J., Demopoulos, G., 2011. Hydrothermal reaction chemistry and characterization of ferric arsenate phases precipitated from Fe2(SO4)3-As2O5-H2SO4 solutions. Hydrometallurgy 107, 74–90.
Gomez, M., Ventruti, G., Celikin, M., Assaaoudi, S., Putz, H., Becze, L., Lee, K.E., Demopoulos, G.P., 2013. The nature of synthetic basic ferric arsenate sulfate (Fe(AsO4)1-x(SO4)x(OH)x) and basic ferric sulfate (FeOHSO4): their crystallographic, molecular and electronic structure with applications in environment and energy. RSC Adv. 3, 16840–16849.
Gunaratnam, A.A., Dreisinger, D., Choi, Y., 2018. Characterisation of solid phases in the iron–sulphate–water system where silver is present. Can. Metall. Q. 57 (4), 405–415.
Larson, A.C., Von Dreele, R.B., 2004. General Structure Analysis System (GSAS). Los Alamos National Laboratory Report LAUR, Los Alamos, USA, pp. 86–748.
Li, J., Sun, J., 2017. Applications of X-ray diffraction and electron crystallography for solving complex structure problems. Acc. Chem. Res. 50 (11), 2737–2745.
Madejova, J., Gates, W.P., Petit, S., 2017. Chapter 5-IR spectra of clay minerals. Dev. Clay Sci. 8, 107–149.
McCreadie, H., Jambor, J.L., Blowes, D.W., Ptacek, C., Hiller, D., 1998. Geochemical behaviour of autoclave-produced ferric arsenate and jarosite in a gold-mine tailings impoundment. In: Petruk, W. (Ed.), Waste Characterization and Treatment. Society for Mining, Metallurgy and Exploration, Littleton, CO, pp. 61–78.
McCreadie, H., Blowes, D.W., Ptacek, C.J., Jambor, J.L., 2000. Influence of reduction reactions and solid-phase composition on porewater concentrations of arsenic. Environ. Sci. Technol. 34 (15), 3159–3166.
McKeown, D.A., 2005. Raman spectroscopy and vibrational analysis of albite: from 25 °C through the melting temperature. Am. Mineral. 90, 1506–1517.
Nan, X.Y., Cai, X., Kong, J., 2014. Pretreatment process on refractory gold ores with As. ISIJ Int. 54 (3), 543–547.
Ojima, J., 2003. Determination of crystalline silica in respirable dust samples by infrared spectrophotmetry in the presence of interferences. J. Occup. Health 45, 94–103.
Paktunc, D., Dutrizac, J.E., 2003. Characterization of arsenate for sulfate substitution in synthetic jarosite using X-ray diffraction and X-ray absorption spectroscopy. Can. Mineral. 41, 905–919.
Paktunc, D., Majzlan, J., Palatinus, L., Dutrizac, J., Klementova, M., Poirier, G., 2013. Characterization of ferric arsenate-sulfate compounds: implications for arsenic control in refractory gold processing residues. Am. Mineral. 98, 554–565.
Powers, D.A., Rossman, G.R., Schugar, H.J., Gray, H.B., 1975. Magnetic behavior and infrared spectra of jarosite, basic iron sulfate, and their chromate analogs. J. Solid State Chem. 13, 1–13.
Reyes, I.A., Patino, F., Flores, M.M., Pandiyan, T., Cruz, R., Gutierrez, E.J., Reyes, M., Flores, V.H., 2017. Dissolution rates of jarosite-type compounds in H2SO4 medium: a kinetic analysis and its importance on the recovery of metal values from hydrometallurgical wastes. Hydrometallurgy 167, 16–29.
Robins, R.G., Jayaweera, L.D., 1992. Arsenic in gold processing. Min. Process. Extr. Metall. Rev. 9, 255–271.
Sasaki, K., Ootsuka, K., Tozawa, K., 1994. Hydrometallurgical studies on hydrolysis of ferric sulphate solutions at elevated temperatures. III. The effect of addition of magnesium sulphate on hydrolysis of ferric sulphate solutions at elevated temperatures. Shigen Sozai 110 (8), 643 in Japanese.
Savage, K.S., Bird, D.K., O'Day, P.A., 2003. Arsenic speciation in synthetic jarosite. Chem. Geol. 215 (1–4), 473–498.
Spratt, H.J., Rintoul, L., Avdeev, M., Martens, W.N., 2013. The crystal structure and vibrational spectroscopy of jarosite and alunite minerals. Am. Mineral. 98 (10), 1633–1643.
Swash, P., Monhemius, A., 1994. Hydrothermal precipitation from aqueous solutions containing iron(III), arsenate and sulphate. Hydrometallurgy 94, 177–190. New York.
Toby, B.H., 2001. EXPGUI, a graphical user interface for GSAS. J. Appl. Crystallogr. 34, 210–213.
Twidwell, L.G., 2019. Treatment of effluent waste. In: Dunne, R.C., Kawatra, S., Young, C.A. (Eds.), SME Mineral Processing and Extractive Metallurgy Handbook. Society for Mining, Metallurgy and Exploration, pp. 1157–1178.
Ugarte, F.J.G., Monhemius, A.J., 1992. Characterization of high temperature arsenic containing residues from hydrometallurgical processes. Hydrometallurgy 30, 69–86.
Ventruti, G., Scordari, F., Shiugaro, E., Gualtieri, A.F., Meneghini, C., 2005. The order–disorder character of FeOHSO4 obtained from the thermal decomposition of metahohmannite, Fe32+ (H2O)4[O(SO4)2]. Am. Mineral. 90, 679–686.
Ventruti, G., Della Ventura, G., Gomez, M.A., Capitani, G., Sbroscia, M., Sodo, A., 2020. High-temperature study of basic ferric sulfate, FeOHSO4. Phys. Chem. Miner. 47 (43) https://doi.org/10.1007/s00269-020-01113-7.
Wang, X., Qin, W., Jiao, F., Yang, C., Cui, Y., Li, W., Zhang, Z., Song, H., 2019. Mineralogy and pretreatment of a refractory gold ore deposit in Zambia. Minerals 9, 406. https://doi.org/10.3390/min9070406.
Yaozhong, L., Smith, R.W., 2004. Arsenic removal from high arsenic bearing gold sulphide concentrate. Miner. Process. Extr. Metall. 113 (3), 189–191.